Journal of ELECTRONIC MATERIALS, Vol. 48, No. 5, 2019
https://doi.org/10.1007/s11664-019-07089-7

Asphalt-Decomposed Carbon-Coated SnO_2 as an Anode for Lithium Ion Batteries

GUODONG LIANG,[1] XIAOGANG SUN,[1,2,3] JIAMEI LAI,[1] CHENGCHENG WEI,[1] YAPAN HUANG,[1] HAO HU,[1] JINGYI ZOU,[1] and YUHAO XU[1]

1.—School of Mechantronics Engineering, Nanchang University, Nanchang 330031, China. 2.—NanoCarbon Co. Ltd, Nanchang 330052, China. 3.—e-mail: xiaogangsun@163.com

In this paper, a SnO_2@C composite anode was prepared by coating SnO_2 with asphalt by hydrothermal process and carbonization. The core–shell structure of SnO_2 nanoparticles was characterized by scanning electron microscopy, energy-dispersive spectrometry, x-ray diffraction and thermal gravimetric analysis. The electrochemical performance tests showed the SnO_2@C anode exhibited excellent cycle performance and high specific capacity. The core–shell structure can accommodate the huge volume expansion of SnO_2 nanoparticles during charge/discharge. The conductivity of the electrode was also obviously enhanced. The first-charge capacity and coulombic efficiency reached 1798 mAh/g and 65%, respectively. After 80 cycles, the capacity still remained at 446 mAh/g at a current density of 100 mA/g.

Key words: SnO_2, asphalt, coating, lithium ion battery, anode

INTRODUCTION

Lithium ion batteries (LIBs) are widely used to power portable electronics and electric vehicles (EVs). It is impending to develop LIBs of high energy density with both long cycling life and highly power output to meet increasing demands.[1–4] Nowadays, it is well known that graphite is widely used for anode materials in commercial LIBs. However, the lower specific capacity of graphite anodes (theoretical capacity of 372 mAh/g) blocks the way for further development of high-performance LIBs. Therefore, finding alternative anode materials for LIBs has become a focus of research in recent years. Owing to the high theoretical specific capacity, metal oxides have been considered as a potential candidate for high-capacity LIBs. Many studies have been done. Among them, SnO_2 exhibits promise as a candidate because of the low cost, environmental friendliness and high theoretical specific capacity (782 mAh/g).[5,6] However, SnO_2 experiences a big volume change of nearly 300% during lithiation and delithiation, which causes severe pulverization of anode materials and results in poor cycling stability and rate capability.[7,8]

An effective way to solve the volume expansion problem of SnO_2 is to introduce carbonaceous materials to modify SnO_2. Many works have been done to improve the performance of SnO_2-based anodes. Coating SnO_2 with carbon is a simple and effective way to enhance the performance of SnO_2. A carbon layer not only accommodates the volume expansion, but also improves the conductivity of the electrodes.[9–12] A variety of carbon materials have been employed to coat SnO_2 for performance enhancement such as glucose, starch and dopamine.[13–17]

Herein, we report a water-soluble asphalt as a carbon source to coat the SnO_2 anode. Compared with other carbon sources, asphalt is cheap and readily available. In addition, asphalt is a carbon compound with low crystallinity and is easy to graphitize.[18,19] Our works showed SnO_2 coated by asphalt to form a core–shell structure (Fig. 1). The surface carbon layer prevented SnO_2 from directly contacting the electrolyte and avoided embedding of

(Received November 27, 2018; accepted February 20, 2019; published online March 6, 2019)

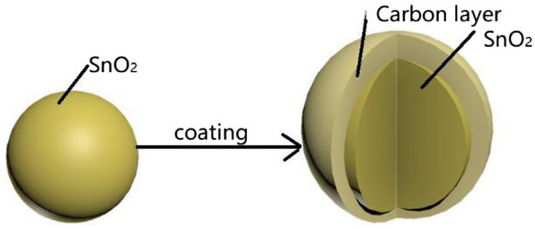

Fig. 1. Structure of SnO_2@C.

solvent molecules to the electrode. The surface carbon layer also improved the electric conduction of the electrode and accommodated the volume expansion to relieve stress.

EXPERIMENTAL

1. Preparation of SnO_2

All chemicals were analytical grade and used without any purification. In this synthesis procedure, 0.01 mol $SnCl_4{\cdot}5H_2O$ was dispersed in 100 ml of deionized water and then magnetically stirred for 10 min to obtain a homogeneous solution. With constant stirring, $NH_3{\cdot}H_2O$ was dripped into the solution to adjust the pH of the suspension to 11. After stirring for 3 h, the precursor solution was put in a stainless-steel reactor which was heated to 180°C for 24 h and cooled with the furnace. After centrifugation, SnO_2 powder was dried at 60°C for subsequent applications.

2. Preparation of composite

Water-soluble asphalt (0.5 g) was dissolved in deionized water to form a 10 wt.% solution. Then 1 g of obtained SnO_2 was impregnated in the asphalt solution with constant stirring for 8 h at room temperature. Then the whole vessel was moved into an oven and dried under 100°C for removing the deionized water to obtain a core–shell structure of asphalt/SnO_2 precursor. The obtained product was kept in a tube furnace at 550°C for 4 h in argon atmosphere to achieve the designed SnO_2@C anode composite.

3. Preparation of coin cell batteries

To evaluate the electrochemical properties of the SnO_2@C composite, CR2025 coin cells were assembled in a glove box filled with Ar gas. A mixture of 80 wt.% SnO_2@C, 10 wt.% conducting agent (Super-P carbon black) and 10 wt.% polyvinylidene fluoride (PVDF) binder were added to N-methyl-2-pyrrolidone (NMP) to form a uniform slurry. After 2 h of mechanical stirring, the slurry was coated onto copper foil with the thickness of 100 μm. After drying at 60°C for 48 h in the vacuum box, the cells were assembled with metal lithium as the counter and polyethylene film (Celgard 2300) as the separator. The electrolyte comprises 1 M LiPF6 in ethyl carbonate (EC)/dimethyl carbonate (DMC)/ethyl methyl carbonate (EMC) at a ratio of 1:1:1 by volume.

4. Materials characterization and the electrochemical measurements

The structures of the composites were characterized by x-ray diffraction (XRD) and Raman spectroscopy. Scanning electronic microscopy (SEM) was also used to observe the size and the morphology of the samples. Thermogravimetric analysis (TGA) was performed to confirm the content of carbon in the composite anode. The galvanostatic charge and discharge test, electrochemical impedance spectroscopy (EIS) and cyclic voltammetry (CV) were performed to evaluate the electrochemical performance.

RESULTS AND DISCUSSION

The prepared SnO_2@C composite is characterized by XRD results in Fig. 2a. All intensive diffraction peaks are well indexed to crystalline SnO_2 (JCPDS card no. 41-1445).[20] The sharp peaks indicate that the SnO_2 powders have high crystallinity. Carbonization did not contribute to the degree of crystallization of SnO_2 NPs as shown in Fig. 2b. In addition, we don't see other peaks on the graph, indicating that no other substances were formed during the synthesis. Moreover, the XRD results also confirm that the carbothermal reduction of SnO_2 to Sn was not triggered below the carbonization temperature of 600°C.[20–23]

Figure 2b shows the Raman spectrum of SnO_2@C with λ_0 = 514 nm. As can be seen from the figure, two main peaks appearing at 1375 cm^{-1} and 1596 cm^{-1} correspond to the D(SP^3) and G(SP^2) bands of carbon, respectively. The results show that asphalt formed an amorphous carbon layer on the surface of SnO_2 after carbonization at 550°C. The ratio of I_D/I_G of 0.75 indicated the presence of a small amount of graphited carbon in the carbon layer.

TGA was performed to determine the carbon content in the SnO_2@C composite, and the result is shown in Fig. 3. It can be observed that the weight loss mainly occurs below 600°C. The temperature is unlikely to cause carbothermal reduction of SnO_2. The carbon content of SnO_2@C composite was calculated at about 34.5 wt.%.

The surface morphologies and structures of SnO_2 and SnO_2@C composites are presented in Fig. 4. Figure 4a shows an SEM image of pure SnO_2. SnO_2@C is exhibited in Fig. 4b, c. Asphalt-coated

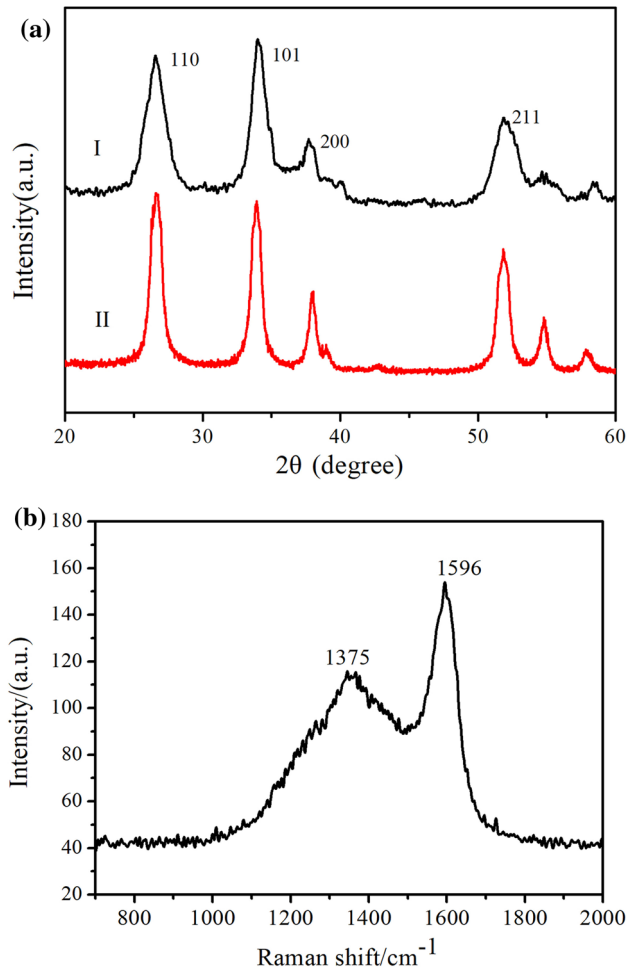

Fig. 2. (a) X-ray diffraction patterns of pure SnO_2 (I) and SnO_2@C composite (II); (b) Raman spectrum of SnO_2@C.

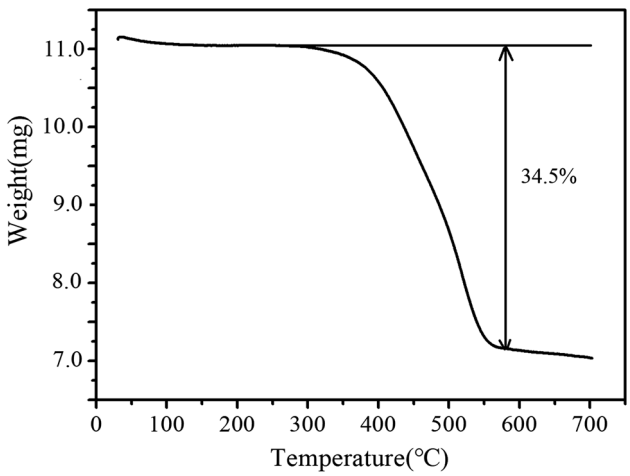

Fig. 3. Thermogravimetric analysis of the SnO_2@C composite.

SnO_2 shows a spheroids structure. The energy-dispersive spectrometer (EDS) images (Fig. 4d) also show the carbon element was uniformly distributed on the surface of SnO_2.

The reaction mechanism of the SnO_2/Li cell includes two steps:[24,25]

$$SnO_2 + 4Li^+ + 4e^- \rightarrow Sn + 2Li_2O \quad (1)$$

$$Sn + xLi^+ + xe^- \leftrightarrow Li_xSn \quad (0 \le x \le 4.4). \quad (2)$$

In order to evaluate the electrochemical performance of the SnO_2@C anode, cyclic voltammetry (CV) measurements were taken at a scan rate of 0.1 $mV \cdot s^{-1}$ in the potential window of 0.01–3 V. The first three cycles of SnO_2@C electrode are shown in Fig. 5. During the first cathodic scan, a strong peak at about 0.75 V is observed, which is attributed to the formation of a solid electrolyte interface (SEI) and the reductive transformation of SnO_2 to Sn and Li_2O as described in reaction 1.[26] It was generally considered to be an irreversible reaction that results in large irreversible capacity losses.[13] The reduction peak disappears during the second and third cycles, indicating that the formation of the SEI and the irreversible process mainly happen during the first cycle. The peak at 0.1 V during the cathodic scan and 0.5 V during the anode scan are attributed to the alloying and dealloying given by reaction 2. The peak at 1.26 V during the first anodic sweep may be a process of partial reversible reaction to form SnO_2. Furthermore, the CV curves of the second and third cycles have a high degree of coincidence, indicating that the charge/discharge paths are basically the same, implying good cyclability of the SnO_2@C anode. Furthermore, the relevant plateau region observed from the initial three charge/discharge profiles of the SnO_2@C electrode (Fig. 6a) is consistent with the peaks of the CV curves.

Figure 6a shows the charge/discharge curves for the SnO_2@C anode and SnO_2 anode after the 1st, 2nd and 10th cycles at a constant current density of 100 mA/g. The profiles of the SnO_2@C are similar to SnO_2 (Fig. 6b). The initial discharge and charge capacities of the SnO_2@C anode reached 1798 mAh/g and 1168 mAh/g, respectively, with an initial coulomb efficiency of 65%. The discharge capacities of the 2nd cycle (1226 mAh/g) and the 10th cycle (898 mAh/g) remained higher than the SnO_2 anode. During the first charge/discharge, the SnO_2@C anode showed a large capacity loss. This is mainly due to the irreversible reaction 1 and the formation of an SEI.[27]

The cycling performance of the SnO_2@C electrode is shown in Fig. 6c. It's obvious that SnO_2@C shows a lower decay rate than the SnO_2 electrode. The SnO_2@C electrode is still able to deliver a reversible capacity of 446 mAh/g after 80 cycles at 100 mA/g, which is higher than the theoretical capacity of graphite (372 mAh/g).

The cycling performance of the SnO_2 electrode is also shown in Fig. 6c. The capacity of the SnO_2 anode decayed to 314 mAh/g and 96 mAh/g after 30 and 80 cycles, respectively. The results show that

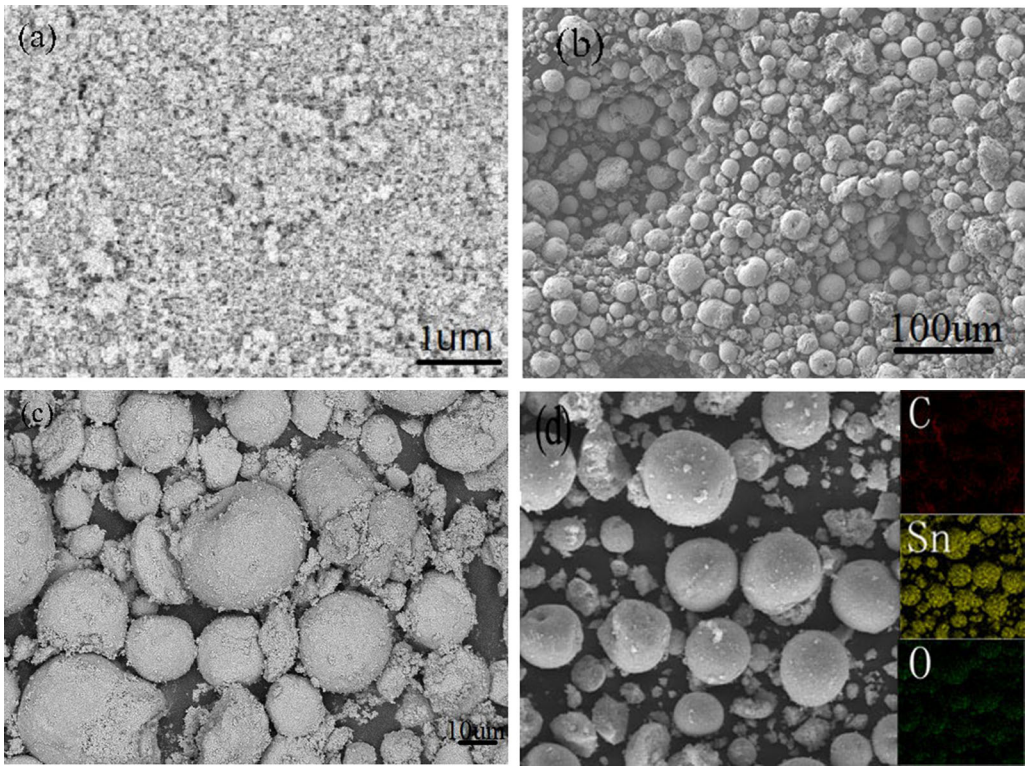

Fig. 4. (a) SEM image of SnO_2 and (b, c) SnO_2@C. (d) EDS image of SnO_2@C.

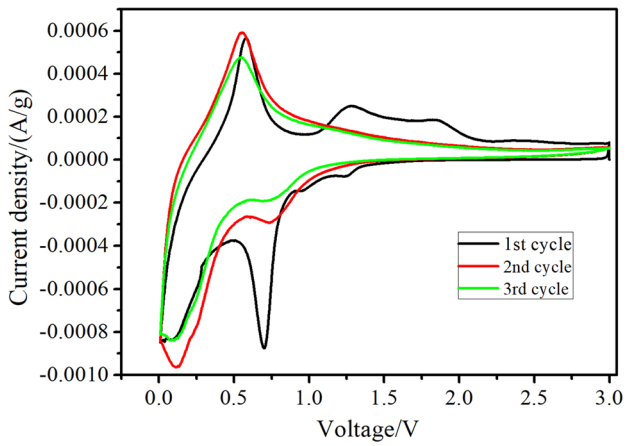

Fig. 5. CV curves of SnO_2@C after the first three cycles.

the introduction of carbon coating to modify SnO_2 accommodated significant volume expansion and relieved the pulverization of anodes. The cycle life of the electrode was enhanced significantly.

Figure 6d demonstrates the rate performance of the SnO_2@C anode. The capacity held at 137.25 mAh/g at 1200 mA/g, but recovered to 396 mAh/g while the current was reduced to 100 mA/g after more than 200 cycles.

In order to investigate the effect of the amorphous carbon layer on the kinetics of Li^+ insertion and deintercalation, electrochemical impedance spectroscopy (EIS) tests were performed. The EIS curves for SnO_2 and SnO_2@C electrodes are shown in Fig. 7. The intercept of the starting point of the semicircle and the horizontal axis represents the migration impedance (*Rs*) of Li^+ in the electrolyte. The semicircular diameter of the high-frequency region indicates the impedance *Rct* caused by the charge transfer in the electrode. The sloping line in the low-frequency region reflects the Warburg impedance of Li^+ in the electrode.[28,29] As shown in Fig. 7, the SnO_2@C electrode has a lower *Rct* than the SnO_2 electrode, which means that the carbon coating layer has an impact on improving the charge transfer impedance in the SnO_2@C electrode during cycling. The electrical resistivity of the SnO_2@C electrode was measured using a four-point probe resistivity tester. The resistivity of SnO_2@C decreased to 0.123 Ω cm compared as 93 Ω cm of SnO_2. The improvement of electrochemical performance can be attributed to the good electrical conductivity of the carbon coating, higher Li^+ transfer kinetics and lower charge transfer resistance.[30–32]

From the above tests and analyses, it can be confirmed that the presence of an amorphous carbon outer layer alleviated the press of volume expansion and pulverization of SnO_2 during the process of Li^+ insertion/extraction. The carbon coating layer also

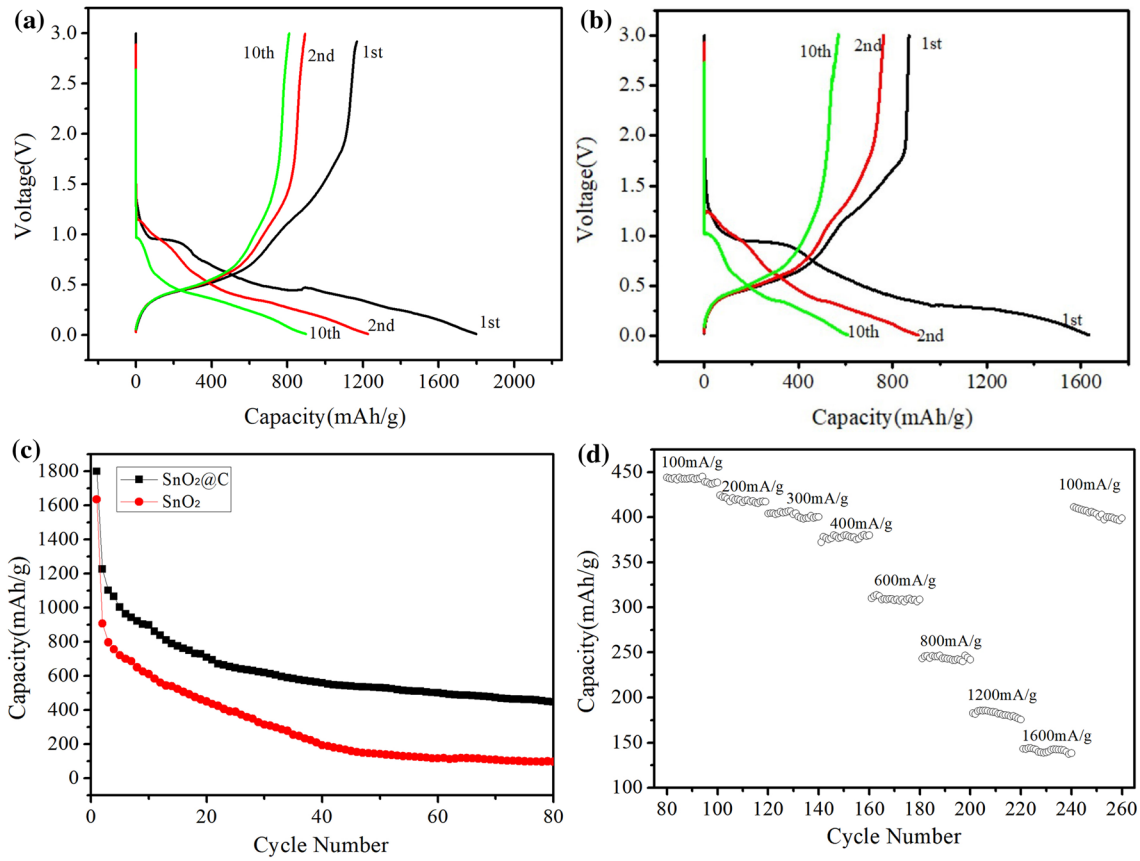

Fig. 6. (a) Charge/discharge voltage profiles of SnO_2@C composite and (b) SnO_2 at a current rate of 100 mA/g. (c) Cyclic performance of the SnO_2@C anode and SnO_2 at a current of 100 mA/g. (d) Rate performance of SnO_2@C.

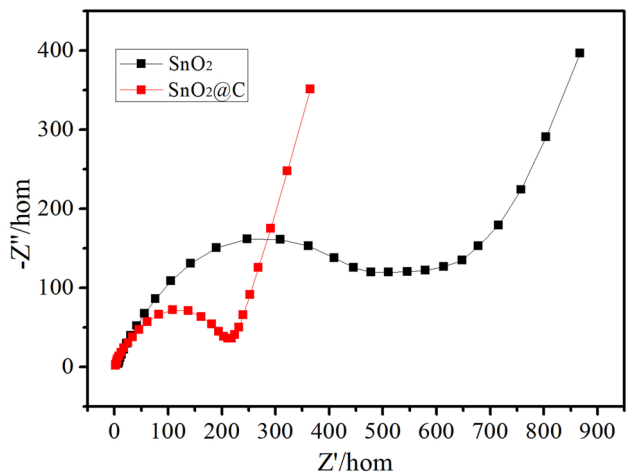

Fig. 7. Electrochemical impedance spectra of SnO_2@C and SnO_2.

improves the conductivity of the anode and electrochemical performance of SnO_2.

CONCLUSION

In summary, we successfully prepared the SnO_2@C composite by a simple two-step process of hydrothermal reaction and carbonization. The carbon-coated SnO_2@C electrode showed better cycle and rate performance than the SnO_2 electrode. After 80 cycles, the capacity of SnO_2@C was maintained at 486 mAh/g at a current density of 100 mA/g. The electrode still exhibited a good electrochemical performance at a high rate of charging and discharging. Our work demonstrated that asphalt can be used as a promising carbon source for coating SnO_2 for practical applications.

FUNDING

This study was funded by the Jiangxi scientific fund (20142BBE50071) and Jiangxi education fund (KJLD13006).

CONFLICT OF INTEREST

We declare that we do not have any commercial or associative interest that represents a conflict of interest in connection with the work submitted.

REFERENCES

1. N.L. Panwar, S.C. Kaushik, and S. Kothari, *Renew. Sust. Energ. Rev.* 15, 1513 (2011).
2. I. Dincer, *Renew. Sust. Energ. Rev.* 4, 157 (2000).
3. J.M. Tarascon and M.B. Armand, *Nature* 414, 359 (2001).
4. V. Etacheri, R. Marom, R. Elazari, G. Salitra, and D. Aurbach, *Energy Environ. Sci.* 4, 3243 (2011).
5. X.W. Lou, Y. Wang, C. Yuan, J.Y. Lee, and L.A. Archer, *Adv. Mater.* 18, 2325 (2006).
6. J.S. Chen and X.W. Lou, *Small* 9, 1877 (2013).

7. D. Larcher, S. Beattie, M. Morcrette, K. Edstrom, J.-C. Jumas, and J.M. Tarascon, *J. Mater. Chem.* 17, 3759 (2007).
8. H. Wang and A.L. Rogach, *Chem. Mater.* 26, 123 (2014).
9. H. Wang, L.F. Cui, Y. Yang, H.S. Casalongue, J.T. Robinson, Y. Liang, Y. Cui, and H. Dai, *J. Am. Chem. Soc.* 132, 13978 (2010).
10. Y.S. Hu, R. Demir-Cakan, M.M. Titirici, J.O. Muller, R. Schlogl, M. Antonietti, and J. Maier, *Angew. Chem. Int. Ed.* 47, 1645 (2008).
11. G. Derrien, J. Hassoun, S. Panero, and B. Scrosati, *Adv. Mater.* 19, 2336 (2007).
12. L. Miao, J. Wu, J. Jiang, and P. Liang, *J. Phys. Chem. C* 117, 23 (2013).
13. J.S. Chen, Y.L. Cheah, Y.T. Chen, N. Jayaprakash, S. Madhavi, and Y.H. Yang, *J. Phys. Chem. C* 113, 20504 (2009).
14. J. Liang, X.Y. Yu, H. Zhou, H.B. Wu, S. Ding, and X.W.D. Lou, *Angew. Chem.* 126, 13017 (2015).
15. H.Q. Wang, J.J. Ji, X. Zhao, J.J. Zhang, Y. Li, Q.Y. Li, and Y.G. Huang, *Mater. Rev.* 27, 48 (2013).
16. T. Xia, W. Zhang, Z. Wang, Y. Zhang, X. Song, J. Murowchick, V. Battaglia, G. Liu, and X.B. Chen, *Nano Energy* 6, 109 (2014).
17. X. Yang, R.Y. Zhang, X.F. Bie, C.Z. Wang, M.L. Li, N. Chen, Y.G. Wei, G. Chen, and F. Du, *Chem. Asian J.* 10, 2460 (2015).
18. H. Lu, B. Liu, G. Chu, J.Y. Zheng, F. Luo, X.P. Qiu, H. Liu, F. Liu, S. Feng, W. Chen, H. Li, and L.Q. Chen, *Energy Storage Sci. Technol.* 5, 109 (2016).
19. Z.Y. Liu, L.K. Liu, X. Jin, H. Tang, and R.G. Sun, *Acta Mater. Compos. Sin.* 36, 141 (2018).
20. X.W. Lou, J.S. Chen, P. Chen, and L.A. Archer, *Chem. Mater.* 21, 2868 (2009).
21. X. Sun, J. Liu, and Y. Li, *Chem. Mater.* 18, 3486 (2006).
22. X.W. Lou, D. Deng, J.Y. Lee, and L.A. Archer, *Chem. Mater.* 20, 6562 (2008).
23. X.W. Lou, C.M. Li, and L.A. Archer, *Adv. Mater.* 21, 2536 (2009).
24. M.S. Park, G.X. Wang, Y.M. Kang, D. Wexler, S.X. Dou, and H.K. Liu, *Angew. Chem.* 46, 750 (2010).
25. R. Demir-Cakan, Y.S. Hu, M. Antonietti, J. Maier, and M.M. Titirici, *Chem. Mater.* 20, 1227 (2008).
26. L. Noerochim, J.Z. Wang, S.L. Chou, H.J. Li, and H.K. Liu, *Electrochim. Acta* 56, 314 (2011).
27. M. Winter, J.O. Besenhard, M.E. Spahr, and P. Novak, *Adv. Mater.* 10, 725 (2010).
28. M.M. Rahmana, J.Z. Wang, M.F. Hassan, S. Chou, D. Wexler, and H.K. Liu, *J. Power Sources* 195, 4297 (2010).
29. Z. Zhou, Y. Xu, W. Liu, and L. Niu, *J. Alloys Compd.* 493, 636 (2010).
30. A.Y. Shenouda and K.R. Murali, *J. Power Sources* 176, 332 (2008).
31. Y. Yao, J. Zhang, L. Xue, T. Huang, and A. Yu, *J. Power Sources* 196, 10240 (2011).
32. K. Wijeratne, J. Akilavasan, M. Thelakkat, and J. Bandara, *Electrochimica Acta* 72, 192 (2012).